Taylor & Francis
Taylor & Francis Group

Combustion Theory and Modelling

ISSN: 1364-7830 (Print) 1741-3559 (Online) Journal homepage: http://www.tandfonline.com/loi/tctm20

Diesel flame lift-off stabilization in the presence of laser-ignition: a numerical study

Cheng Gong, Mehdi Jangi & Xue-Song Bai

To cite this article: Cheng Gong, Mehdi Jangi & Xue-Song Bai (2015): Diesel flame lift-off stabilization in the presence of laser-ignition: a numerical study, Combustion Theory and Modelling, DOI: 10.1080/13647830.2015.1077997

To link to this article: http://dx.doi.org/10.1080/13647830.2015.1077997

Published online: 21 Sep 2015.

Submit your article to this journal

Article views: 59

View related articles

View Crossmark data

Full Terms & Conditions of access and use can be found at
http://www.tandfonline.com/action/journalInformation?journalCode=tctm20

Download by: [Lund University Libraries] **Date:** 25 November 2015, At: 01:40

Combustion Theory and Modelling, 2015
http://dx.doi.org/10.1080/13647830.2015.1077997

Taylor & Francis
Taylor & Francis Group

Diesel flame lift-off stabilization in the presence of laser-ignition: a numerical study

Cheng Gong*, Mehdi Jangi and Xue-Song Bai

Division of Fluid Mechanics, Department of Energy Sciences, Lund University, Lund, Sweden

(*Received 15 April 2015; accepted 15 July 2015*)

Diesel flame lift-off and stabilization in the presence of laser-ignition were numerically investigated with the method of Eulerian stochastic fields. The aim was to scrutinise the interaction between the lifted diesel flame and an ignition kernel upstream of the lifted flame. The numerical simulation was carried out in a constant-volume combustion vessel with *n*-heptane as fuel. The process was studied previously in an experiment employing Diesel #2 as the fuel in the same combustion vessel. In the experiment a lifted flame was first established at a position downstream of the nozzle. An ignition kernel was then initiated using a high-energy pulse laser at a position upstream of the natural lift-off position of the diesel flame. The laser-ignition kernel was modelled using a high-temperature (∼2000 K) hot spot. In both experiment and simulations the upstream front of the ignition kernel was shown to remain around the initial laser ignition site for a substantially long period of time, while the downstream front of the ignition kernel propagates rapidly towards the natural lift-off position downstream of the laser ignition site. The lift-off position oscillated before the final stabilization at the natural lift-off position. The structures and the propagation speed of the reaction fronts in the laser-ignition kernel and the main flame were analysed. Two different stabilization mechanisms, the auto-ignition mechanism and the flame propagation mechanism, were identified for the naturally lifted flame and the laser-induced reaction front, respectively. A mechanism was proposed to explain the oscillation of the lift-off position.

Keywords: diesel combustion; flame stabilization; auto-ignition; laser ignition; Eulerian stochastic fields method

Downloaded by [Lund University Libraries] at 01:40 25 November 2015

1. Introduction

The reaction zone of a diesel jet flame is typically stabilised at a location downstream of the fuel injector. The process of the reaction zone's finding its natural stabilisation position is referred to as the *lift-off* of a diesel flame. The lifted flame allows for the fuel and the ambient air to mix in the upstream of the reaction zone, which can affect the combustion and the soot formation process [1]. Owing to its importance in industrial applications, lifted flames have been studied extensively. In particular, lifted turbulent gaseous jet flames have been investigated by many authors under atmospheric conditions. Various theories have been proposed to explain the stabilisation mechanism of the lifted flames [2, 3], for example, reaction front propagation at the flame base [4], local extinction due to high scalar dissipation rate [5], and vortex/flame interaction [6].

When the ambient temperature is sufficiently high, for example, under diesel engine conditions, the fuel/air mixture can auto-ignite. To understand the combustion process

*Corresponding author. Email: Cheng.Gong@energy.lth.se; Fax: +46462224717

© 2015 Taylor & Francis

in diesel engines, a number of experiments have been carried out in constant-volume combustion chambers under engine relevant thermochemical conditions. For example, the Engine Combustion Network (ECN) [7] provides a list of experimental cases under different fuel and ambient conditions. In these experiments, the importance of auto-ignition in the lift-off process under diesel engine combustion conditions has been evidenced, for example the cool flame (first-stage ignition) in the upstream of the lift-off position [8–10] and the shorter lift-off lengths for fuels with shorter ignition delay times [8, 11]. Despite these findings, the mechanisms for lift-off and stabilisation in diesel spray flames are as yet debatable. For example, a cool flame may either enhance flame propagation or lead directly to second-stage ignition [8]. Moreover, the lift-off heights and the reaction-zone structures of spray flames depend on the ambient conditions and the injections. For example, two different structures of the flame base were found under different conditions in both experiments [11] and simulations [12].

Another evidence of the importance of auto-ignition in the lift-off is the detached ignition kernels upstream of the lift-off position in diesel sprays [8, 11]. Pauls *et al*. [11] discussed the periodic appearance of detached ignition kernels upstream of the lift-off position: the detached ignition kernels, which move towards and merge with the downstream main flame, are later followed by the onset of detached new ignition kernels upstream of the flame. The lifted flame appears to fluctuate around a 'quasi-steady' lift-off position. To investigate the effect of detached ignition kernels upstream of the natural lift-off position in a diesel flame, Pickett *et al*. [13] experimentally studied the problem in a constant-volume combustion vessel. In their experiment, an ignition kernel in the region upstream of the lift-off position was generated using a high-energy pulsed laser. The ignition kernel was shown to sustain near the ignition site for a substantially long period of time before moving towards and merging with the main flame downstream. Based on the experimental results, Pickett *et al*. [13] offered a potential mechanism for the transient lift-off response to laser ignition based on turbulent mixing with the high-temperature combustion product at the jet edges. However, due to the limited experimental data several questions could not be answered, e.g. the effect of the laser ignition on the low-temperature chemistry zone (the cool flame) and the stabilisation mechanism for the laser-induced ignition kernel.

Computational fluid dynamics (CFD) has been shown to be a powerful tool in recent research on diesel spray combustion. Reviews of recent numerical work on diesel combustion can be found in [14–16]. The traditional approach of CFD to the diesel spray is to model the gas phase by the Eulerian method and the liquid phase by the particle-based Lagrangian method. In diesel sprays, the liquid fuel is injected at very high speed, which generates strong turbulence in the combustion chamber. Limited by computation cost, most numerical studies of diesel sprays have been based on the unsteady Reynolds-averaged Navier–Stokes (URANS) method coupled with simplified turbulent combustion models, e.g. the well-stirred reactor (WSR) model [17, 18] or flamelet type models [19, 20]. Recently, the transported probability density function (PDF) model based on the Lagrangian stochastic particle method coupled with URANS [14, 15] and large-eddy simulation (LES) [21] have been used for diesel spray simulation. By comparing the results from the WSR and transported PDF models, it was shown [15] that the two models predicted significantly different turbulent flame structures. The PDF model predicted a more distributed turbulent flame brush, which was more consistent with that observed in experiment.

Another method to solve the transported PDF of the reactive scalar is the Eulerian stochastic fields (ESF) method [22], in which the reactive scalars are solved using a set of stochastic differential equations. The ESF method is easier to couple with the conventional CFD code compared with the usually used Lagrangian stochastic particle method. Jones

Downloaded by [Lund University Libraries] at 01:40 25 November 2015

et al. have demonstrated the LES/ESF method in gas-jet [23, 24] and spray-combustion [25, 26] simulations.

In the present work, the laser-induced ignition process in the constant-volume combustion vessel studied by Pickett *et al*. [13] is simulated using the ESF method to gain insights into the detailed structures of the reaction fronts in the presence of an ignition kernel upstream of a lifted diesel flame. The aim is to delineate the characteristics of the reaction fronts and the interaction between the ignition kernel and the lifted flame.

2. Modelling methodology

2.1 *Numerical models for spray combustion*

In this study, the spray flow and combustion process are modelled using a coupled Eulerian–Lagragian approach. The gas phase is described in the Eulerian frame with the unsteady Reynolds-averaged Navier–Stocks (URANS) equations and the standard $k-\varepsilon$ model for turbulence. In the two-equation $k-\varepsilon$ model, the turbulence kinetic energy k and its rate of dissipation e are obtained from the following transport equations:

$$\frac{\partial \bar{\rho} k}{\partial t} + \bar{\rho}\tilde{u}_i \frac{\partial k}{\partial x_i} = \frac{\partial}{\partial x_i}\left(\frac{\mu_t}{\sigma_k}\frac{\partial k}{\partial x_i}\right) + G - \bar{\rho}\varepsilon \tag{1}$$

$$\frac{\partial \bar{\rho} \varepsilon}{\partial t} + \bar{\rho}\tilde{u}_i \frac{\partial \varepsilon}{\partial x_i} = \frac{\partial}{\partial x_i}\left(\frac{\mu_t}{\sigma_\varepsilon}\frac{\partial \varepsilon}{\partial x_i}\right) + \frac{\varepsilon}{k}(C_1 G - C_2 \bar{\rho}\varepsilon) \tag{2}$$

with the turbulent viscosity calculated as

$$\mu_t = \bar{\rho} C_\mu \frac{k^2}{\varepsilon}, \tag{3}$$

where G represents the generation rate of turbulence kinetic energy due to the mean velocity gradient; $C_1 = 1.44$, $C_2 = 1.92$, $C_\mu = 0.09$, $\sigma_k = 1.0$, and $\sigma_\varepsilon = 1.3$ are the model constants. In asymmetric jet flows, an increased value for C_1 was suggested to predict the jet spread [27]. A previous study [28] showed that with the modified value $C_1 = 1.53$, better agreement with experiment was obtained in terms of spray penetration. Similar conclusions have been reported in other numerical simulations under the same conditions [14, 29].

The liquid phase is modelled with discrete parcels whose motion is described using the Lagrangian particle tracking (LPT) approach. Each parcel represents a group of spherical droplets whose position, size, and physical properties are similar. Gas and liquid phases are coupled through the mass, momentum, and heat-exchange source terms between the phases. OpenFOAM® [30] is used for the numerical integration of the governing equations. Further details about the governing equations and the spray sub-models can be found in [31, 32].

In the ESF method, the turbulent reactive flows are represented by N_F stochastic fields. The governing equation for the nth stochastic field is

$$\begin{aligned}\bar{\rho}\,\mathrm{d}\phi_\alpha^{(n)} = &-\bar{\rho}\tilde{u}_i \frac{\partial \phi_\alpha^{(n)}}{\partial x_i}\,\mathrm{d}t + \bar{\rho} S_\alpha^r(\Phi^{(n)})\,\mathrm{d}t + \bar{\rho} S_\alpha^s(\Phi^{(n)})\,\mathrm{d}t \\ &+ \frac{\partial}{\partial x_i}\left(\Gamma_t \frac{\partial \phi_\alpha^{(n)}}{\partial x_i}\right)\mathrm{d}t - \frac{1}{2}\bar{\rho} C_\phi(\phi_\alpha^{(n)} - \tilde{\phi}_\alpha)\omega_t\,\mathrm{d}t + \bar{\rho}\sqrt{2\frac{\Gamma_t}{\bar{\rho}}}\frac{\partial \phi_\alpha^{(n)}}{\partial x_i}\,\mathrm{d}W_i^{(n)},\end{aligned} \tag{4}$$

Downloaded by [Lund University Libraries] at 01:40 25 November 2015

where ϕ_α can be the mass fraction of species (Y_i) or the enthalpy of the mixture (h), and $\Phi^{(n)} = [Y_1^{(n)}, \ldots, Y_{Ns}^{(n)}, h^{(n)}]$. $\Gamma_t = \mu_t/\sigma_t$ is the turbulent diffusivity, where μ_t is the turbulent viscosity and σ_t is the turbulent Schmidt number in the transport equations for chemical species or the Prandtl number in the enthalpy equation. $\bar{\rho} S_\alpha^r(\Phi^{(n)})\,\mathrm{d}t$ and $\bar{\rho} S_\alpha^s(\Phi^{(n)})\,\mathrm{d}t$ are the source term increments due to the chemical reactions and the spray evaporation, respectively.

The term involving C_ϕ in Equation (4) represents the molecular mixing, which is modelled using the *Interaction with Exchange to the Mean* (IEM) model, and ω_t is the turbulence frequency obtained from $\omega_t = \varepsilon/k$ with k and ε being the turbulent kinetic energy and its dissipation rate. $\mathrm{d}\boldsymbol{W}^{(n)}$ represents a vector Wiener process that is spatially uniform but different for each field. The mixing-model constant C_ϕ is set as 2.5, which is referenced to the Lagrangian PDF simulation [14] under similar conditions. The mean and the moments of each variable can be approximated from the ensemble of N_F stochastic fields. For example, the mean is

$$\tilde{\phi}_\alpha = \frac{1}{N_F} \sum_{n=1}^{N_F} \phi_\alpha^{(n)}. \tag{5}$$

An operator-splitting algorithm is used to integrate the chemical source terms in Equation (4). To integrate the source terms due to chemical reactions efficiently, a recently developed acceleration method, the so-called chemistry-coordinate mapping (CCM) method [33, 34], is employed. The basic idea of the CCM method is to map the thermo-chemistry identical cells in the physical space to a multidimensional phase space. In general, there are multiple physical cells mapped to one phase space zone, which results in a speed-up of the numerical integration of the chemical reaction rates. A four-dimensional phase space based on (T, J_H, $\nabla J_\mathrm{H} \cdot \nabla J_\mathrm{H}$, J_fuel) was used in the present simulations. Here, J_H is the mass fraction of the hydrogen element; $\nabla J_\mathrm{H} \cdot \nabla J_\mathrm{H}$ is analogous to the scalar dissipation rate. A previous study [35] with the same kinetic mechanism showed that the speed-up for the chemical source term integration was about 25 when a stabilised flame is estimated. Details about the ESF-CCM method can be found in [35].

2.2 *Experimental configuration and simulation setups*

The experiment carried out by Pickett *et al*. [13] is considered in the present study. The reacting spray in this experiment was generated in the constant-volume vessel of the ECN [7] with Diesel #2 fuel. A laser-induced plasma ignition was applied at a position upstream of the natural lift-off position in the spray flame. In the present study, the ambient and injection conditions, which are listed in Table 1, were obtained from the ECN database [7] with a similar ignition delay time and lift-off length to those in the laser-ignition experiment. The laser-spot was set at the jet edge at the position $x = 20$ mm on the axial coordinate and $r = 1.5$ mm on the radial coordinate, to make sure that it can ignite the local combustible mixture upstream the natural lift-off position. The x–r coordinate is shown in Figure 1. The Bilger's mixture fraction is used to quantify the mixing in the reactive flow field, which is defined as

$$\xi = \frac{2(Y_\mathrm{C} - Y_\mathrm{C}^\mathrm{o})/W_\mathrm{C} + (Y_\mathrm{H} - Y_\mathrm{H}^\mathrm{o})/2W_\mathrm{H} - (Y_\mathrm{O} - Y_\mathrm{O}^\mathrm{o})/W_\mathrm{O}}{2(Y_\mathrm{C}^\mathrm{f} - Y_\mathrm{C}^\mathrm{o})/W_\mathrm{C} + (Y_\mathrm{H}^\mathrm{f} - Y_\mathrm{H}^\mathrm{o})/2W_\mathrm{H} - (Y_\mathrm{O}^\mathrm{f} - Y_\mathrm{O}^\mathrm{o})/W_\mathrm{O}}, \tag{6}$$

Downloaded by [Lund University Libraries] at 01:40 25 November 2015

Table 1. Ambient and injection conditions used in the simulation.

Ambient temperature	850 K
Ambient density	14.8 kg/m^3
Ambient gas composition	O_2, 21 vol.%
N_2, 69.33 vol.%	
CO_2, 6.11 vol.%	
H_2O, 3.56 vol.%	
Injection pressure drop	140 MPa
Nozzle diameter	0.100 mm
Injection flow rate	2.755 mg/ms
Fuel	Diesel #2
Fuel temperature	436 K

Downloaded by [Lund University Libraries] at 01:40 25 November 2015

where Y_C, Y_H, and Y_O are the element mass fractions; W_C, W_H, and W_O are the atomic weights for the elements; the superscript 'o' and 'f' indicate the oxidiser and the fuel stream, respectively. The stoichiometric mixture fraction (ξ_{st}) in the present condition is 0.0609.

A pulsed laser was used to generate the ignition kernel in the experiment. The pulse duration of the laser was 8 ns [13], which is much smaller than the time step involved in the present CFD simulation. The complex process of the initial ignition kernel after the laser pulse is beyond the scope of the present study. Thus, a hot spot with radius 1 mm was used in the simulation to model the initial ignition kernel. Hot spots with temperatures of 1500, 2000, and 2200 K were tested, which will be discussed in Section 3. Finally, a hot spot with temperature 2000 K was adopted based on the sensitivity study. Though the present grid resolution cannot predict the initial development of the hot spot, the turbulent reaction brush is much thicker than the grid size once the ignition kernel induced by the hot spot has formed.

A previous numerical study [28] showed the grid-independence result can be obtained with a grid size of 0.5 mm. A similar 2D-axisymmetric mesh was used in the present

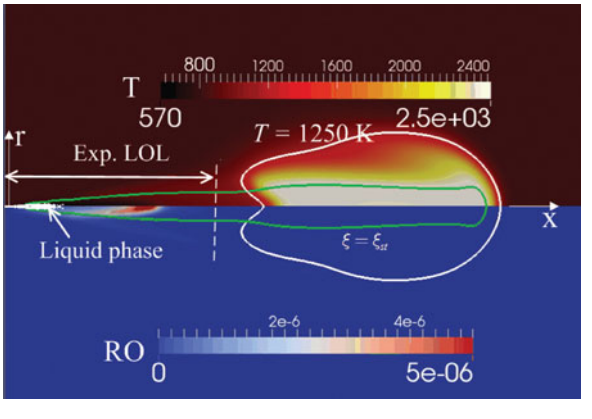

Figure 1. Distributions of the simulated temperature (upper half of the figure) and RO radicals (lower half of the figure) at 3.9 ms ASI; the vertical dashed line shows the lift-off position from the experiment [13]; RO is the total mass fraction of RO-1 and RO-2 shown in Figure 2. The white solid line denotes the iso-contour of $T = 1250$ K; the green solid line denotes the iso-contour of the stoichiometric mixture fraction. (color online)

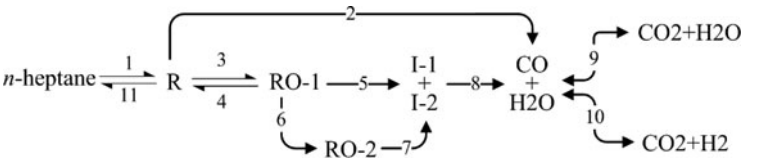

Figure 2. Reaction path for *n*-heptane oxidation according to the global mechanism [37].

simulations. It is uniform on the axial direction with $dz = 0.5$ mm; in the radial direction, it is uniform with $dx = 0.5$ mm within 10 mm from the jet axis and is stretched in the outer domains with a stretch ratio of 1.08. The lifted flame base and the laser-induced ignition kernel were resolved in the uniform region of the mesh. The total number of cells is about 13,000. Twenty stochastic fields were used for the ESF calculation. The chemical kinetic mechanism for Diesel #2 is not well developed; usually it is modelled using *n*-heptane in numerical simulations [36]. Here, a global chemical kinetic mechanism [37] involving 12 species and 11 reactions was adopted to model the chemical reaction. The mechanism was developed for modelling auto-ignition of mixtures of *iso*-octane and *n*-heptane. The mechanism involves five reactions for the high-temperature chemistry and six reactions for the low-temperature chemistry. The reaction path for the *n*-heptane part of the mechanism is shown in Figure 2, where R represents the heptyl radicals, RO-1 and RO-2 represent the oxygenated-heptyl radicals, which branch to smaller radicals, I-1 and I-2, through reaction 5. I-1 and I-2 are then oxidised further to CO and H_2O along with the release of a small amount of heat. RO-1, RO-2, I-1, and I-2 play important roles in the cool flame to be discussed later. It will be shown below that this mechanism can provide comparable ignition delay time and lift-off length to the experiment with Diesel #2 fuel under the present conditions.

3. Results and discussion

Figure 1 shows a snapshot of the gas temperature and the mass fraction of RO at 3.9 ms after the start of injection (ASI); the mass fraction of RO is the sum of the mass fractions of RO-1 and RO-2 shown in Figure 2, which are the key species for the low-temperature chemistry in the mechanism. Typically, OH radicals are used to characterise the high-temperature reaction zone in a diesel flame. OH is however not included in the present chemical kinetic mechanism; thus, the iso-contour of temperature at 1250 K, which is 400 K above of the ambient temperature, is used to identify the high-temperature reaction zone and the lift-off position. The figure shows that the numerical simulation with the present simplified chemical kinetic mechanism captures a lift-off length (LOL) in reasonably good agreement with experiment. At 3.9 ms ASI, which is the time that the laser ignition was applied, the lift-off position in the experiment (shown as the vertical dashed line in Figure 1) is slightly upstream of that from the numerical simulations.

Different temperatures for the hot spot were used to generate the initial ignition kernel in the simulation. The maximum mass fraction of CO_2 in the hot spot and the LOL after the onset of ignition in the hot spot with different initial temperatures are compared in Figure 3. It is shown that the hot spot with an initial temperature of 1500 K failed to ignite the local mixture. The LOL jumped to a much higher value, which corresponds to the natural lift-off position of the lifted flame. Both of the other two hot spots can ignite the local mixture successfully. It is notable that the initial induction time in the two successful

Downloaded by [Lund University Libraries] at 01:40 25 November 2015

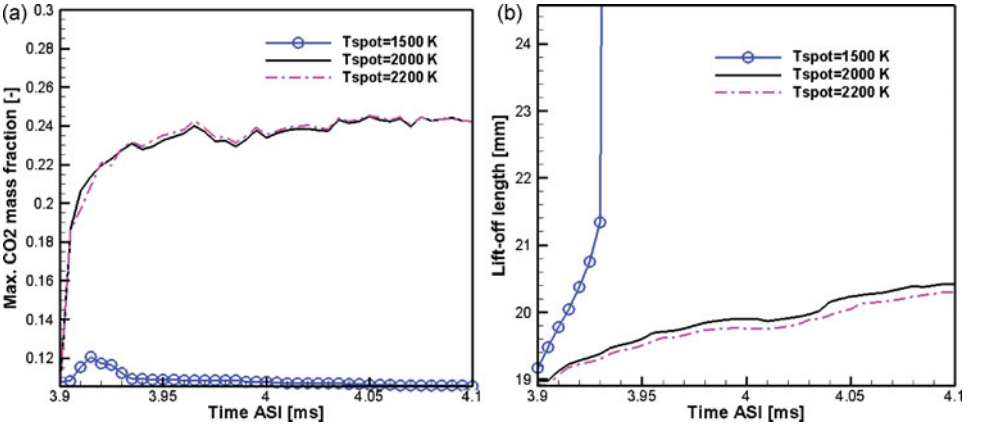

Figure 3. The evolutions of the initial ignition kernel with different temperatures for the initial hot spot: (a) the maximum mass fraction of CO_2 at the ignition kernel; (b) the lift-off length defined based on $T = 1250$ K.

ignition cases (∼0.015 ms) is very much shorter than the whole evolution history of the laser-induced ignition kernel. The LOLs with different hot spot temperatures experienced a similar history, which means the LOLs are insensitive to the initial hot spot temperature. Based on the above sensitivity study, the hot spot with 2000 K was adopted for further simulation.

Figure 4 shows the evolution of the temperature distribution after the initiation of the ignition spot in the simulation and the chemiluminescence images from the experiment. As shown from the simulation and the experiment, the ignition kernel generated by the laser grows in size and propagates downstream quickly. It merges with the original lifted flame at 4.175 ms ASI in the simulation, which is a little later than that in the experiment due to the over-predicted lift-off length in the simulation. An explanation for the rapid propagation of the downstream reaction front is the high-speed convective flow driven by the spray. Although the downstream reaction front of the laser-ignition region moves quickly, the upstream reaction front remains close to the original position by the time the flame merges at the natural lift-off position. At 5.2 ms ASI, the predicted leading front of the merged flame has moved downstream to the axial position around 30 mm, which is consistent with experiment.

Figure 5 shows the LOL before and after the laser ignition from both simulation and experiment. Here, the LOL from simulation is defined as the smallest axial distance between the nozzle and the point at temperatures above 1250 K. It is shown that the lift-off position jumps to the ignition site at the onset of laser-ignition; thereafter, the lift-off position moves downstream towards the natural (without laser ignition) lift-off position. Finally, the lift-off is stabilised at a position close to the natural lift-off position. A comparison between simulation and experiment shows that the present simulation captures all these characteristics of the evolution process of the laser-induced ignition kernel in the experiment qualitatively well, although some discrepancies can be pointed out. The time required for the ignition kernel to stabilise at the natural lift-off position in the simulation is slightly shorter than that in the experiment. It is noteworthy that there was an oscillation before final stabilisation of the lift-off length in the simulation. This process was not found in the experiment with the same laser-shot position. However, a similar oscillation process was found in the experiment with a shorter distance between the laser-shot position and

Downloaded by [Lund University Libraries] at 01:40 25 November 2015

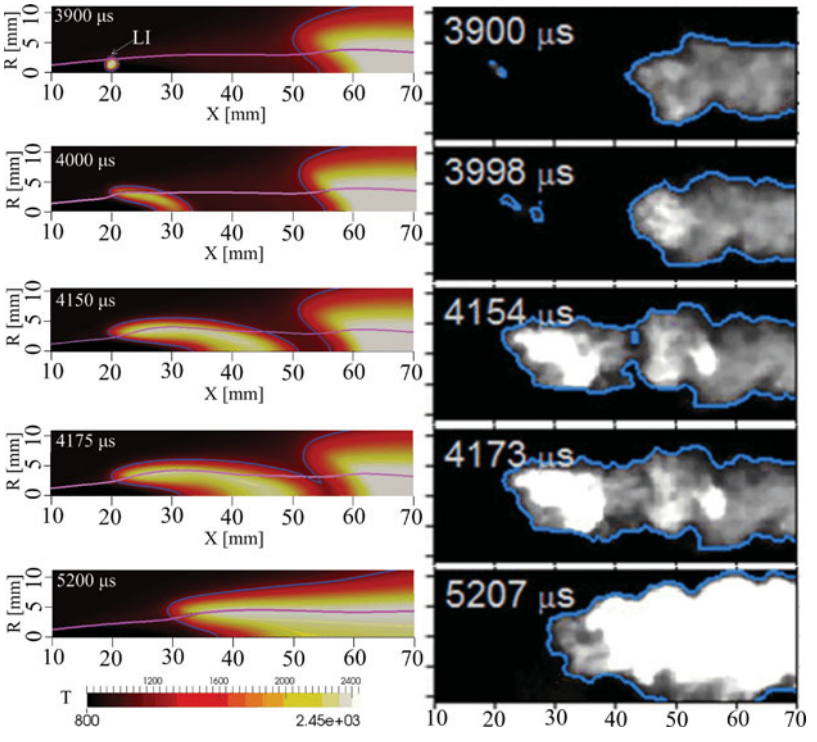

Figure 4. Temperature sequence with laser ignition at 3.9 ms ASI from the numerical simulations (left) and the experimental chemiluminescence images (right) [13]. Experimental data for comparison was reprinted from Proc. Comb. Inst., 32 (2009), L.M. Pickett *et al.*, Diesel fuel jet lift-off stabilization in the presence of laser-induced plasma ignition, P2796, Copyright (2009), with permission from Elsevier. The blue lines in the left column are the iso-contours of 1250 K; the pink lines are the iso-contours of the stoichiometric mixture fraction. (color online)

the natural lift-off position (see the dashed curve in Figure 5). A possible reason for the absence of the oscillation process in the experiment with laser-ignition set at $x = 20$ mm is that the lift-off position moved back to the natural position around 10 ms ASI, which is at the end of the fuel injection; after that the whole flame was blown out. This oscillation process might be useful for understanding the oscillation of the LOL with the appearance of auto-ignition events upstream of the lift-off position, which will be discussed later.

Figure 6 shows the distributions of temperature and key species at 4.0 and 4.175 ms ASI with and without the laser-ignition. It is shown that in both the main flame and the laser-ignition kernel the low-temperature chemistry species (RO and I in Figure 6) disappeared. These species are for the low-temperature chemistry path, which ends when the temperature is high and the high-temperature path becomes dominant. RO is seen in a small region around the axis of spray. Radicals I are seen in the same region of RO but also in a larger region downstream. From the heat release distribution, one can see that the consumption of RO and I is associated with a relative low level of heat release (as compared with the high-temperature main flame region downstream). This low-temperature heat release zone is referred to as the cool flame, which is seen to increase the temperature in front of the main flame, cf. Figures 4 and 6. The numerical results shown in Figure 6 indicate that the laser ignition does not affect the temperature distribution due to the cool

Downloaded by [Lund University Libraries] at 01:40 25 November 2015

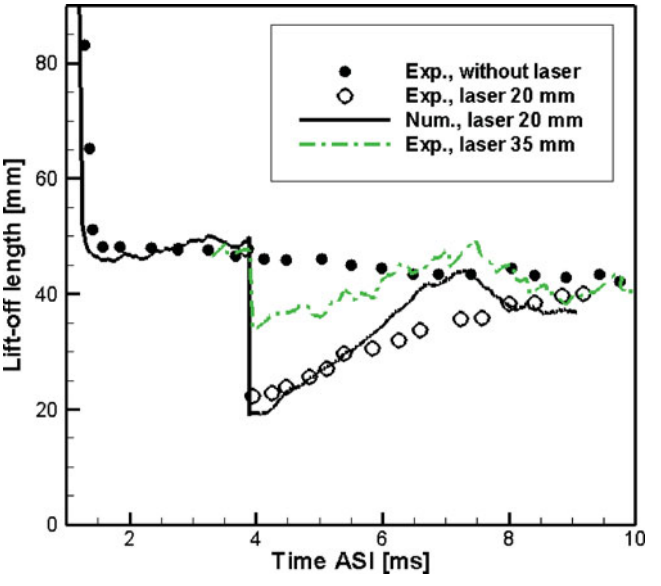

Figure 5. Evolution of the lift-off length with and without laser ignition. Experimental data was reprinted from Proc. Comb. Inst., 32 (2009), L.M. Pickett *et al.*, Diesel fuel jet lift-off stabilization in the presence of laser-induced plasma ignition, P2796, Copyright (2009), with permission from Elsevier.

Downloaded by [Lund University Libraries] at 01:40 25 November 2015

flame. The main flame downstream of the laser ignition kernel is essentially identical at the two instants of time shown in Figure 6. The primary effect of the laser ignition is to enlarge the main flame in the axial direction (cf. Figure 4) when the laser-ignition-induced small flame merges with the main flame.

To investigate the mechanisms of propagation of the laser-induced reaction front and the natural lifted flame, the budget terms of the diffusion transport term and the reaction rate term in the transport equation for the mass fraction of CO_2 were examined. It has been argued previously [38, 39] that when the diffusion term is significantly smaller than the reaction rates, the reaction front is essentially an ignition front. At a flame front, the diffusion term and reaction rates should be comparable in their magnitudes.

Figure 7 shows the budget terms across the leading fronts of the laser-ignition-induced reaction zone and the main flame, as well as a 1D unstretched premixed flame. The mean diffusion term and the reaction rate are obtained by applying the ensemble average of the diffusion term and the chemical reaction term in Equation (4) over the stochastic fields. Only turbulent diffusion is considered in the mean diffusion term, which is consistent with the transport equations in the simulations. The 1D premixed flame was computed using an open-source code, Cantera [40], with the same kinetic mechanism as that used in the 2D simulation. Since the ambient temperature (850 K) in the 2D simulation is high enough to lead to the mixture auto-igniting. The unburnt temperature in the 1D free-propagating flame was set as 300 K instead of 850 K. The progress variable in the figure is defined as

$$c = \frac{Y_{\mathrm{CO_2}} - Y^{\mathrm{unb}}_{\mathrm{CO_2}}}{Y^{\mathrm{b}}_{\mathrm{CO_2}} - Y^{\mathrm{unb}}_{\mathrm{CO_2}}}, \tag{7}$$

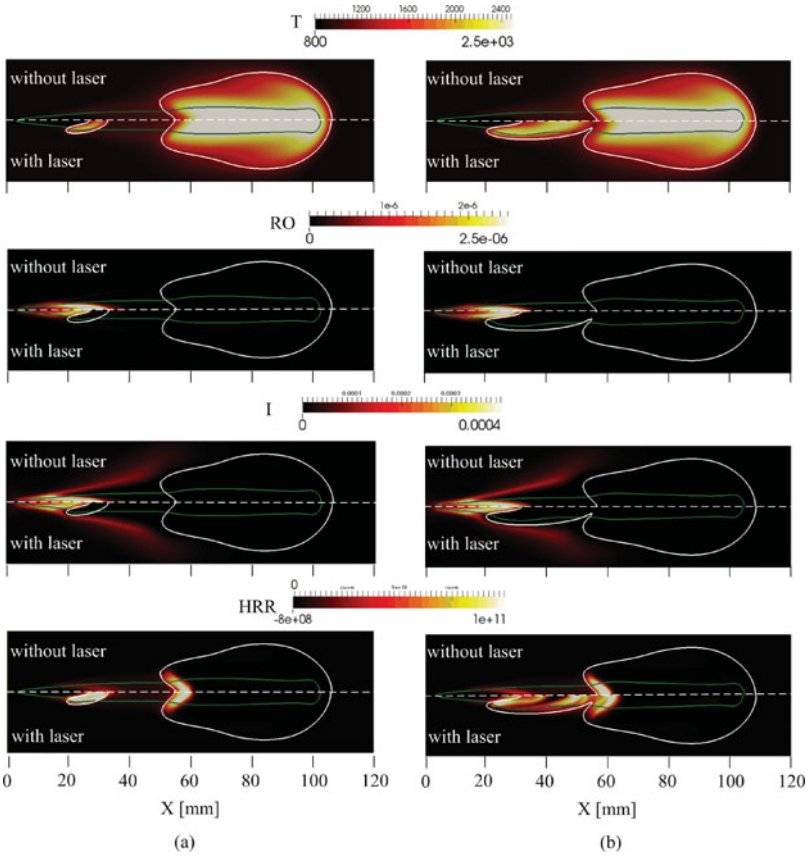

Figure 6. Distributions of the simulated gas temperature, mass fractions of species for the low-temperature chemistry and the local heat-release rate (HRR) with and without laser-ignition at 4.0 ms (a) and 4.175 ms (b) ASI; the mass fraction RO is the total mass fractions of RO-1 and RO-2; the mass fraction of I is the total mass fraction of I-1 and I-2; the solid white lines in the temperature fields are the iso-contours of $T = 1250$ K; the solid green lines denote the stoichiometric mixture fraction; the dashed horizontal lines denote the spray axis. (color online)

where $Y_{CO_2}^{unb}$ and $Y_{CO_2}^{b}$ are the mass fractions of CO_2 in the unburnt and fully burnt mixtures along the local equivalence ratio of unity, respectively. The figure illustrates that, in the 1D premixed flame, the diffusion term has the same order of magnitude as the chemical reaction rate across the flame front. At the position with the highest reaction rate (with the progress variable about 0.8) the diffusion term is about 40% of the reaction rate in magnitude. Across the leading front of the laser-ignition-induced reaction zone (the 'ignition kernel' in Figure 7), the diffusion term is also on the same order as the reaction rate. The ratio of the diffusion term to the reaction rate at the position with the highest reaction rate is about 60%, which indicates that the reaction front is a flame front. Since the oxygen and fuel are partially mixed in front of the reaction zone, it is concluded that the reaction front is a partially premixed flame. From the species distribution shown in Figure 6(a), low-temperature reactions are taking place in front of the flame; hence the flame is an ignition-assisted flame. It was evidenced in the experiment [41] that the presence of low-temperature reactions could increase the turbulent flame speed. A different structure is

Downloaded by [Lund University Libraries] at 01:40 25 November 2015

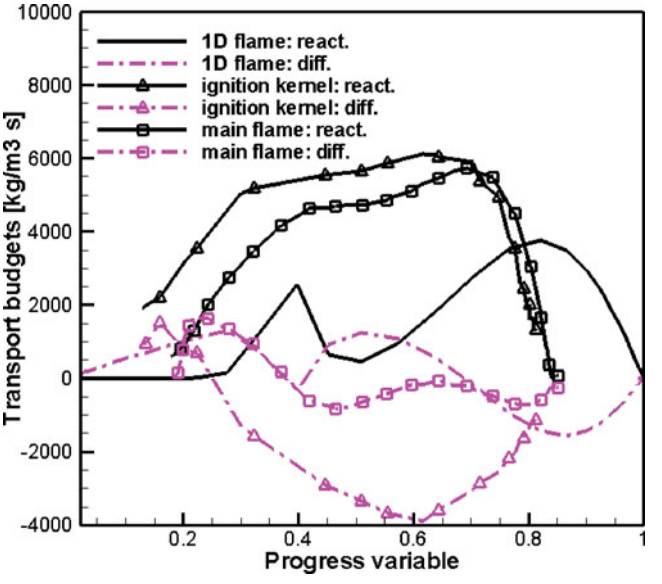

Figure 7. The diffusion term and the reaction rate in the transport equation for the mass fraction of CO_2 at the reaction front for the laser-induced ignition kernel and the main flame. The data from the 2D simulation are sampled across the reaction fronts with the stoichiometric mixture fraction at 4.15 ms ASI; the 1D premixed flame is computed for 300 K and 3.55 MPa, with unity equivalence ratio as the inlet condition.

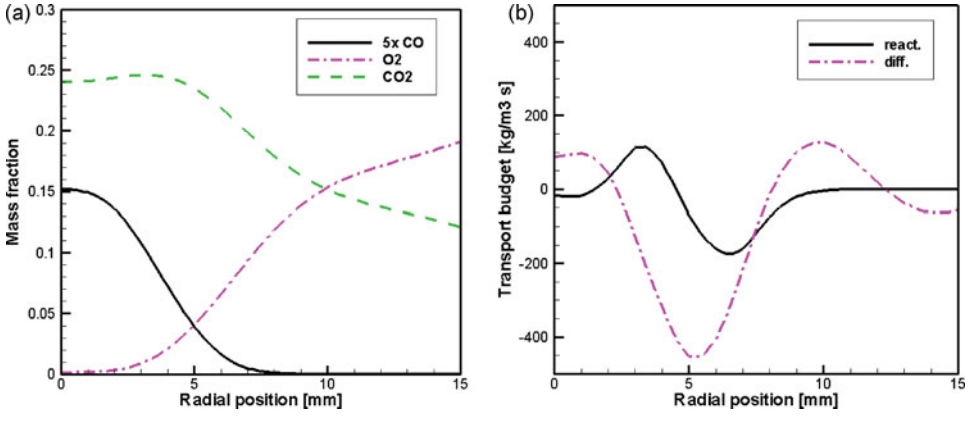

Figure 8. Flame structure at the axial position $x = 75$ mm: (a) distribution of the mass fractions of CO, O_2, and CO_2; (b) diffusion and reaction budgets in the transport equation for CO_2.

found at the reaction front of the downstream lifted flame (the 'main flame' in Figure 7(b)), where the diffusion term is much lower than the reaction rate. The ratio of the diffusion term to the reaction rate at the position with the highest reaction rate is about 10%, which means that it is more similar to an ignition front than a flame front.

Figure 8(a) shows the distributions of O_2, CO, and CO_2 across the main flame along the radial direction at the axial position $x = 75$ mm at 4.15 ms ASI. At these axial positions, the fuel, *n*-heptane, has been converted to combustion intermediates, mainly CO. The peak CO is found in the inner part of the flame around the axis of the spray. CO and O_2 diffuse

Downloaded by [Lund University Libraries] at 01:40 25 November 2015

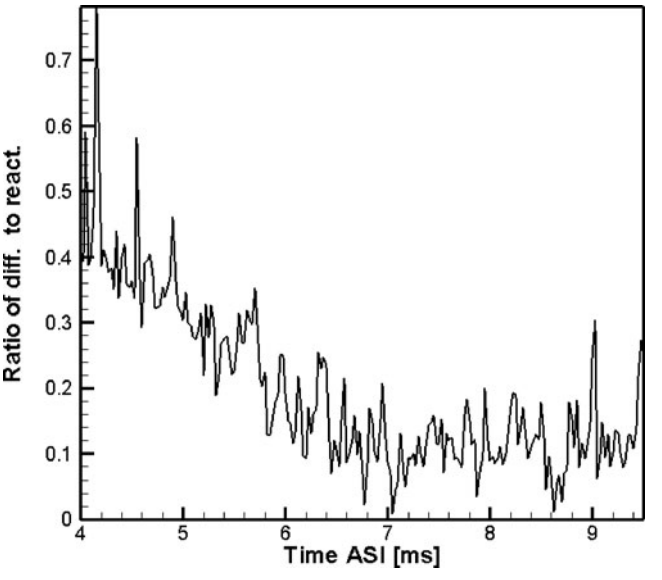

Figure 9. Ratio of the diffusion term to the reaction rate for CO_2 at the flame front with the maximum reaction rate and stoichiometric mixture fraction.

towards each other and react in a thick layer around a radial position of 5 mm, where the mass fraction of CO_2 is relatively higher. This is the well-known diffusion flame structure. Figure 8(b) shows the budget terms in the transport equation for the CO_2 mass fraction at the same locations and the same instant of time as those in Figure 8(a). It is clear that the diffusion term is in the same order of magnitude as that of the chemical reaction rate. From Figures 7 and 8, one can conclude that the main flame is made up of a leading ignition front and a diffusion flame that follows the leading ignition front. The lift-off position and the stabilisation of the main flame are therefore governed by the ignition reactions in the mixture upstream of the main flame.

Since the ratio of the diffusion term to the reaction rate of CO_2 is a parameter to identify the combustion mode at the leading front of the flame, Figure 9 shows this ratio as a function of time ASI after the laser-ignition; the data were sampled at the flame front (defined as the position with the highest reaction rate) with the stoichiometric mixture fraction. It is shown that the ratio decreased from 0.5 to 0.1 from 4.0 to 7.0 ms ASI; thereafter, the ratio fluctuated around 0.1. Based on the above discussion, one can conclude that the reaction front of the upstream laser-ignition kernel switched from the flame mode to the ignition mode with the increase of the LOL.

Similar to some direct numerical simulation (DNS) work [38, 39], the displacement speed of the turbulent flame brush can be calculated based on an iso-surface of a chosen value of a chosen species (here the mass fraction of CO_2 is chosen). The displacement speed of the flame brush is defined as

$$S_{\mathrm{d}} = \left(-\frac{\mathrm{D}\tilde{Y}_{\mathrm{CO_2}}}{\mathrm{D}t} \left| \nabla \tilde{Y}_{\mathrm{CO_2}} \right|^{-1} \right) \Bigg|_{\tilde{Y}_{\mathrm{CO_2}} = Y_{\mathrm{CO_2,\,ref}}}, \tag{8}$$

where $Y_{\mathrm{CO_2,\,ref}}$ is a reference mass fraction of CO_2 to define the turbulent flame brush of the high-temperature reaction zone. $Y_{\mathrm{CO_2,\,ref}} = 0.2$ is used in the present discussion. This

Downloaded by [Lund University Libraries] at 01:40 25 November 2015

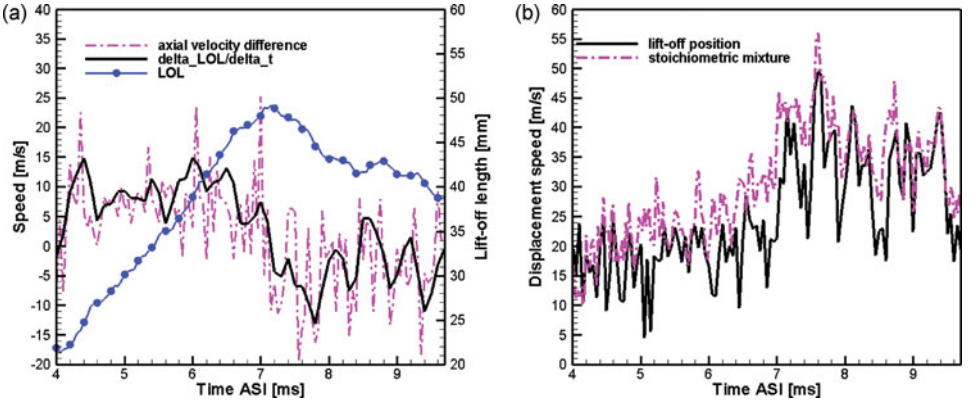

Figure 10. (a) velocity difference at the lift-off position as well as the time derivative of lift-off length (LOL); (b) local displacement speeds at the lift-off position and the flame front with a stoichiometric mixture; the lift-off position in this figure is defined as the position with the minimum axial distance to the nozzle on the iso-contour of $Y_{CO_2} = 0.2$.

value corresponds to a progress variable of about 0.6 for the stoichiometric mixture. The difference between the local displacement speed and the local velocity along the normal direction of a reaction front can be defined as

$$\triangle u = \vec{\tilde{u}} \cdot \vec{n}_f - s_{d,f} \quad \text{with} \quad \vec{n}_f = \nabla \tilde{Y}_{CO_2} \Big/ \left|\nabla \tilde{Y}_{CO_2}\right|, \tag{9}$$

where $\vec{n}_f$ is the unit vector normal to the reaction front. If the velocity difference were zero, the reaction front would be stabilised at its previous location. In addition, the axial component of the velocity difference can be defined as

$$\Delta u_x = (\vec{n}_f \cdot \vec{n}_x)\Delta u, \quad \text{with} \quad \vec{n}_x = (1, 0), \tag{10}$$

where $\vec{n}_x$ is the unit vector on the axial direction.

The axial component of the velocity difference at the lift-off position and the LOL are shown in Figure 10(a). Here, the lift-off position is defined as the position with the minimum axial distance to the nozzle on the iso-surface of $Y_{CO_2} = Y_{CO_2,\,\mathrm{ref}}$. The velocity difference shown in the figure indicates that the iso-surfaces of the CO_2 mass fraction are moving in the flow field. The axial component of the velocity difference fluctuated around 10 m/s before 7.0 ms; during this period the LOL increased almost linearly with time. Thereafter, the axial component of the velocity difference jumped to negative values, which corresponded to upstream shifting of the lift-off position. The axial component of velocity difference fluctuated around zero, finally. The time derivative of LOL within $\triangle t = 1.0$ ms is plotted in Figure 10(a). Here, the time derivative is another way to evaluate the velocity difference at the leading reaction front. The time derivative of the LOL has a similar distribution to that of the velocity difference between the local displacement speed and local velocity, cf. Figure 10(a). The local displacement speed at the lift-off position is shown in Figure 10(b). Since the mixture fraction (or equivalence ratio) at the lift-off position might change with time, the local displacement speed at the flame front with the stoichiometric mixture fraction is plotted in Figure 10(b). It is shown that the local displacement speed at the lift-off position fluctuated with a relatively stable mean value before 7.0 ms ASI. During this period, a slow increase can be identified for the local displacement speed at the

Downloaded by [Lund University Libraries] at 01:40 25 November 2015

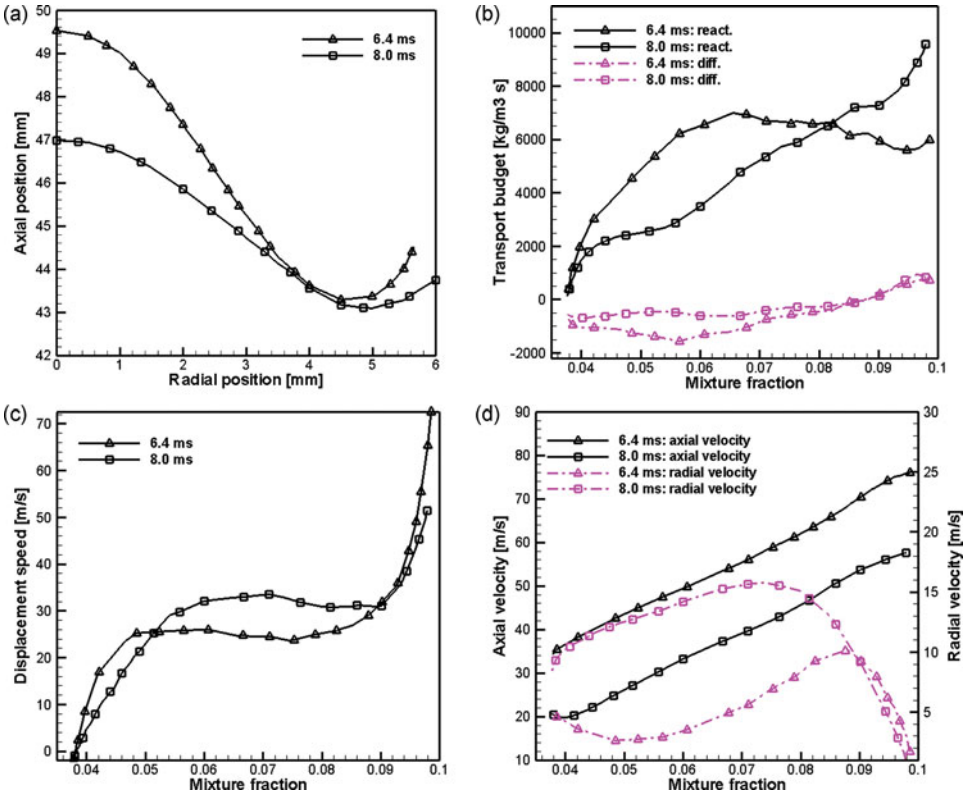

Figure 11. The flow and reaction-zone structures at the flame bases at 6.4 and 8.0 ms ASI; (a) the shapes of the flame bases; (b) the diffusion term and the reaction rate in the transport equation for the mass fraction of CO_2; (c) the local displacement speed; (d) the velocity components. The flame bases are defined as $Y_{CO_2,\,ref} = 0.2$.

stoichiometric mixture, which can be explained by the increased fuel concentration (or the mixture fraction) gradient: the displacement speed of a partially premixed flame decreases with the fuel concentration gradient [42, 43]. The fuel concentration gradient decreases with the axial position in the jet. The displacement speeds increased to a higher level of around 7.0 ms ASI in Figure 10(b). As shown in Figure 9, after 7 ms ASI auto-ignition had been the dominant mechanism for flame stabilisation.

Based on Figure 10, one can discover that, before the leading reaction front shifted to the auto-ignition mode, the displacement speed of the reaction front was smaller but comparable to the local convection velocity on the normal direction. This indicates that the slow downstream propagation of the reaction front is a flame controlled process. This is different from the argument in [13], which assumed that the stabilisation of the leading reaction front is due to the mixing of the hot product to the front; as such, local turbulence promoted turbulent flame propagation.

As mentioned above, there was an oscillation process before final stabilisation of the LOL (see Figures 5 and 10(a)). Flow fields at 6.4 and 8.0 ms ASI were chosen to examine the oscillation process. At these two instants of time, the lifted flame had almost the same LOL (about 43 mm in Figure 10(a)) but different directions of propagation of the lift-off position. The flow and reaction-zone structures at the flame bases are shown in Figure 11.

Downloaded by [Lund University Libraries] at 01:40 25 November 2015

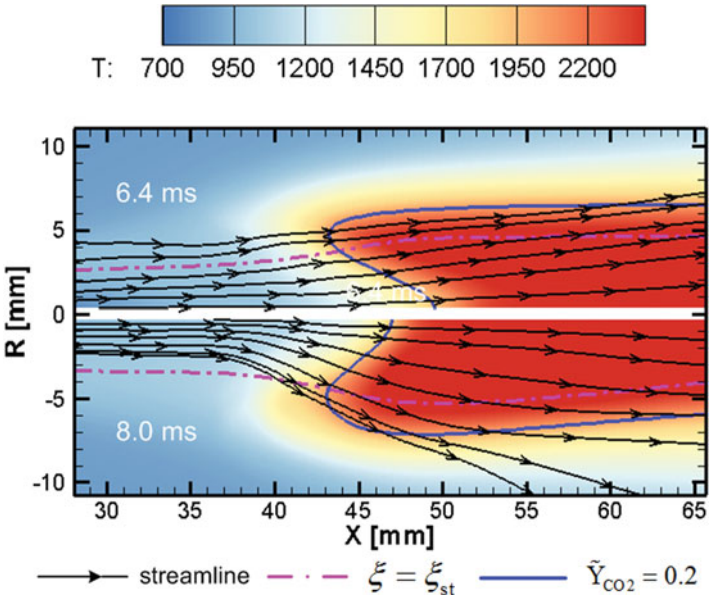

Figure 12. The streamline around the flame bases at 6.4 and 8.0 ms ASI.

The spatial locations of the flame bases shown in Figure 11(a) reveal that the widths of the flame bases are almost the same; the curvature at 8.0 ms ASI is lower than that at 6.4 ms ASI. Additionally, the mixture fractions on the jet axis (the maximum mixture in Figures 11(b)–11(d)) are almost the same, which implies a similar mixing field on the flame bases at these two instants of time. The transport budgets of the reaction rate and diffusion terms for the mass fraction of CO_2 are shown in Figure 11(b). At 6.4 ms ASI, the highest reaction rate on the flame base was located around the stoichiometric mixture. The highest reaction rate shifted to the fuel-rich mixture at 8.0 ms ASI. This implies that the reaction on the inner side of the flame base played a more important role in flame stabilisation at this instant of time. The local displacement speeds on the flame bases are shown in Figure 11(c). It can be noted that the displacement speed around the lift-off position (with the mixture fraction varying between 0.055 and 0.07) at 8.0 ms is higher than that at 6.4 ms ASI. This might contribute to the lower curvature at 8.0 ms ASI, since the local displacement speed decreases with flame curvature [44]. The local velocity on the flame bases is shown in Figure 11(d). The axial velocity is almost linearly increasing with the local mixture fraction for both of the flame bases. For the mixture with the same equivalence ratio (the mixture fraction) and the same progress variable (the mass fraction of CO_2), the axial velocity at 8.0 ms ASI is about 15 m/s lower than that at 6.4 ms ASI, while the radial velocity at 8.0 ms ASI is lower than that at 6.4 ms ASI. The effect of the flame bases on the flow field can also be found in the streamline shown in Figure 12. It is shown that, with the flatter flame base, the flow divergence due to the thermal expansion of the flame base is increased at 8.0 ms ASI. From Figures 9–12, one can conclude that when the dominate mechanism for flame stabilisation is switched from flame propagation to auto-ignition, the reactions on the fuel-rich mixture play a more important role in flame stabilisation; it makes the flame base flatter and decreases the axial flow velocity by increasing the flow divergence upstream of the flame front. As a result, the lift-off position will shift to an upstream position before final stabilisation.

Downloaded by [Lund University Libraries] at 01:40 25 November 2015

Although this study focuses on the evolution of a laser-ignition event, a similar evolution could be experienced when a detached ignition zone is generated in an auto-ignition event. Furthermore, since the increased flow divergence can increase the residence time by reducing the axial velocity, it could promote the onset of a new auto-ignition event upstream of the lift-off position. In this sense, the presently predicted oscillation process for the LOL is consistent with the flame stabilisation process discussed in Pauls *et al*. [11].

4. Conclusions

Diesel flame lift-off and stabilisation in the presence of laser-ignition were numerically investigated with the Eulerian stochastic fields (ESF) method and unsteady Reynolds Averaged Navier–Stokes (URANS) equations. A numerical model for the laser ignition was applied at an upstream position of the natural lift-off position.

The present simulation with the ESF method can capture the evolution of the laser-induced ignition kernel upstream of the natural lift-off position, including the fast propagation of the downstream reaction front, the slow downstream shifting of the leading reaction front of the laser-induced reaction front towards the natural lift-off position of the flame, and the oscillation of the lift-off position before final stabilisation (this feature was not discussed in the previous experimental work [13]). Additional insights were observed from the simulations into the effect of the ignition kernel on the lifted flame. The following conclusions are drawn.

The laser ignition does not affect the temperature distribution due to the cool flame in the upstream of the natural lift-off position. The main effect of the laser ignition is to enlarge the main flame in the axial direction when the laser-ignition-induced small flame merges with the main flame.

The transport budgets of the reaction rate and the diffusion terms at the leading front of the natural lifted flame and the laser-induced flame front were examined. The natural lifted fame is stabilised by auto-ignition under the present conditions, while the reaction front induced by the laser ignition is an ignition-assisted partially premixed flame.

The displacement speed at the flame front was evaluated based on the diffusion and reaction rate budgets. The displacement speed is lower than, but comparable to, the local convection velocity in the normal direction of the reaction front. This displacement speed can stabilise the flame front around the ignition site for a substantial period of time; the flame front moves downstream slowly due to the higher convection velocity in comparison with the local displacement speed.

With the downstream shifting of the lift-off position, the reaction front at the lift-off position switches from the flame mode to the ignition mode. The lifted flame is eventually stabilised by the ignition reactions in the mixture upstream of the lift-off position. When the flame base of the lifted flame switches to auto-ignition, the reactions on the fuel-rich mixture make the flame base flatter, and decrease the incoming flow velocity by increasing the flow divergence of the jet flow. These effects result in an upstream shifting of the lift-off position before final stabilisation.

Acknowledgements

The computations were performed using the computer facilities provided by the Centre for Scientific and Technical Computing at Lund University (LUNARC), the High Performance Computing Center North (HPC2N), and the Center for Parallel Computers (PDC).

Disclosure statement

No potential conflict of interest was reported by the authors.

Downloaded by [Lund University Libraries] at 01:40 25 November 2015

Funding

This work was supported by the Swedish research funding organisations (CeCOST; KCFP; VR). Cheng Gong was sponsored by the China Scholarship Council (CSC).

References

[1] L.M. Pickett and D.L. Siebers, *Soot in diesel fuel jets: effects of ambient temperature, ambient density, and injection pressure*, Combust. Flame 138 (2004), pp. 114–135.
[2] W.M. Pitts, *Assessment of theories for the behavior and blowout of lifted turbulent jet diffusion flames*, Proc. Combust. Inst. 22 (1989), pp. 809–816.
[3] K.M. Lyons, *Toward an understanding of the stabilization mechanisms of lifted turbulent jet flames: experiments*, Prog. Energy Combust. Sci. 33 (2007), pp. 211–231.
[4] T. Gautam, *Lift–off heights and visible lengths of vertical turbulent jet diffusion flames in still air*, Combust. Sci. Technol. 41 (1984), pp. 17–29.
[5] N. Peters and F.A. Williams, *Liftoff characteristics of turbulent jet diffusion flames*, AIAA J. 21 (1983), pp. 423–429.
[6] J.E. Broadwell, W.J.A. Dahm, and M.G. Mungal, *Blowout of turbulent diffusion flames*, Proc. Combust. Inst. 20 (1985), pp. 303–310.
[7] *Engine Combustion Network*. 2014; Available at http://www.sandia.gov/ecn/dieselSprayCombustion.php.
[8] L.M. Pickett, D.L. Siebers, and C.A. Idicheria, *Relationship Between Ignition Processes and the Lift-Off Length of Diesel Fuel Jets*, SAE paper 2005-01-3843 (2005). Available at http://dx.doi.org/10.4271/2005-01-3843.
[9] C.A. Idicheria and L.M. Pickett, *Formaldehyde visualization near lift-off location in a diesel jet*, SAE paper 2006-01-3434 (2006). Available at http://dx.doi.org/10.4271/2006-01-3434.
[10] S.A. Skeen, J. Manin, and L.M. Pickett, *Simultaneous formaldehyde PLIF and high-speed schlieren imaging for ignition visualization in high-pressure spray flames*, Proc. Comb. Inst. 35 (2015), pp. 3167–3174.
[11] C. Pauls, S. Vogel, G. Grunefeld, and N. Peters, *Combined simulations and OH-chemiluminescence measurements of the combustion process using different fuels under diesel-engine like conditions*, SAE paper 2007-01-0020 (2007). Available at http://dx.doi.org/10.4271/2007-01-0020.
[12] C. Gong, M. Jangi, and X.S. Bai, *Large eddy simulation of* n*-dodecane spray combustion in a high pressure combustion vessel*, Appl. Energ. 136 (2014), pp. 373–381.
[13] L.M. Pickett, S. Kook, H. Persson, and Ö. Andersson, *Diesel fuel jet lift-off stabilization in the presence of laser-induced plasma ignition*, Proc. Comb. Inst. 32 (2009), pp. 2793–2800.
[14] Y. Pei, E. Hawkes, and S. Kook, *A comprehensive study of effects of mixing and chemical kinetic models on predictions of* n*-heptane jet ignitions with the PDF method*, Flow Turbul. Combust. 91 (2013), pp. 249–280.
[15] S. Bhattacharjee, and D.C. Haworth, *Simulations of transient* n*-heptane and* n*-dodecane spray flames under engine-relevant conditions using a transported PDF method*, Combust. Flame 160 (2013), pp. 2083–2102.
[16] J. Abraham, *Critical observations on the modeling of nonreacting and reacting diesel sprays*, Proc. Inst. Mech. Engrs, Pt. D: J. Automobile Engng (2015). Available at http://dx.doi.org/10.1177/0954407014565407.
[17] S. Som, D.E. Longman, Z. Luo, M. Plomer, and T. Lu, *Three dimensional simulations of diesel sprays using* n*-dodecane as a surrogate*, Fall Technical Meeting of the Eastern States Section of the Combustion Institute, 9–12 October 2011, Storrs, CT. Available at http://www.researchgate.net/profile/Tianfeng_Lu/publication/267204075_Three_Dimensional_Simulations_of_Diesel_Sprays_Using_n-_Dodecane_as_a_Surrogate/links/546638b30cf25b85d17f5cbf.pdf.
[18] S. Som, Z. Luo, P.K. Senecal, E. Pomraning, M. Plomer, D.E. Longman, and T. Lu, *Simulating flame lift-off characteristics of diesel and biodiesel fuels using detailed chemical-kinetic mechanisms and large eddy simulation turbulence model*, J. Energy Resour. Technol. 134 (2012), pp. 032204–032204.
[19] G. D'Errico, T. Lucchini, F. Contino, M. Jangi, and X.S. Bai, *Comparison of well-mixed and multiple representative interactive flamelet approaches for diesel spray combustion modelling*, Combust. Theory Model. 18 (2014), pp. 65–88.

Downloaded by [Lund University Libraries] at 01:40 25 November 2015

[20] C. Bajaj, M. Ameen, and J. Abraham, *Evaluation of an unsteady flamelet progress variable model for autoignition and flame lift-off in diesel jets*, Comb. Sci. Technol. 185 (2012), pp. 454–472.
[21] A. Irannejad, A. Banaeizadeh, and F. Jaberi, *Large eddy simulation of turbulent spray combustion*, Comb. Flame 162 (2015), pp. 431–450.
[22] L. Valiño, *A field Monte Carlo formulation for calculating the probability density function of a single scalar in a turbulent flow*, Flow Turbul. Combust. 60 (1998), pp. 157–172.
[23] W.P. Jones and S. Navarro-Martinez, *Large eddy simulation of autoignition with a subgrid probability density function method*, Combust. Flame 150 (2007), pp. 170–187.
[24] W.P. Jones and V.N. Prasad, *Large eddy simulation of the Sandia Flame Series (D–F) using the Eulerian stochastic field method*, Combust. Flame 157 (2010), pp. 1621–1636.
[25] W.P. Jones, A.J. Marquis, and K. Vogiatzaki, *Large-eddy simulation of spray combustion in a gas turbine combustor*, Combust. Flame 161 (2014), pp. 222–239.
[26] W.P. Jones, A.J. Marquis, and D. Noh, *LES of a methanol spray flame with a stochastic sub-grid model*, Proc. Combust. Inst. 35 (2015), pp. 1685–1691.
[27] J. Janicka and N. Peters, *Prediction of turbulent jet diffusion flame lift-off using a PDF transport equation*, Symp. (Int.) Combust. 19 (1982), pp. 367–374.
[28] K.M. Pang, M. Jangi, X.-S. Bai, and J. Schramm, *Investigation of chemical kinetics on soot formation event of* n*-heptane spray combustion*, SAE paper 2014-01-1254 (2014). Available at http://dx.doi.org/10.4271/2014-01-1254.
[29] R. Novella, A. García, J.M. Pastor, and V. Domenech, *The role of detailed chemical kinetics on CFD diesel spray ignition and combustion modelling*, Math. Comput. Model. 54 (2011), pp. 1706–1719.
[30] *The OpenFOAM Foundation*. 2015. Available at www.openfoam.org/.
[31] M. Jangi, T. Lucchini, G. D'Errico, and X.S. Bai, *Effects of EGR on the structure and emissions of diesel combustion*, Proc. Comb. Inst. 34 (2013), pp. 3091–3098.
[32] C. Gong, M. Jangi, T. Lucchini, G. D'Errico, and X.-S. Bai, *Large eddy simulation of air entrainment and mixing in reacting and non-reacting diesel sprays*, Flow Turbul. Combust. 93 (2014), pp. 385–404.
[33] M. Jangi, R. Yu, and X.S. Bai, *A multi-zone chemistry mapping approach for direct numerical simulation of auto-ignition and flame propagation in a constant volume enclosure*, Combust. Theory Model. 16 (2011), pp. 221–249.
[34] R. Solsjö, M. Jangi, C. Chartier, Ö. Andersson, and X.S. Bai, *Lift-off and stabilization of n-heptane combustion in a diesel engine with a multiple-nozzle injection*, Proceedings of the Combustion Institute 34 (2013), pp. 3031–3038.
[35] M. Jangi, T. Lucchini, C. Gong, and X.-S. Bai, *Effects of fuel cetane number on the structure of diesel spray combustion: An accelerated Eulerian stochastic fields method*, Combust. Theory Model. (2015). Doi:10.1080/13647830.2015.1057234
[36] S.C. Kong, Y. Sun, and R.D. Rietz, *Modeling diesel spray flame liftoff, sooting tendency, and NOx emissions using detailed chemistry with phenomenological soot model*, Journal of Engineering for Gas Turbines and Power 129 (2007), pp. 245–251.
[37] S. Voglsam, and F. Winter, *A global combustion model for simulation of n-heptane and iso-octane self ignition*, Chem. Eng. J. 203 (2012), pp. 357–369.
[38] R. Yu, and X.S. Bai, *Direct numerical simulation of lean hydrogen/air auto-ignition in a constant volume enclosure*, Combust. Flame 160 (2013), pp. 1706–1716.
[39] J.H. Chen, E.R. Hawkes, R. Sankaran, S.D. Mason, and H.G. Im, *Direct numerical simulation of ignition front propagation in a constant volume with temperature inhomogeneities: I. Fundamental analysis and diagnostics*, Combust. Flame 145 (2006), pp. 128–144.
[40] *Cantera: chemical kinetics, thermodynamics, transport processes*. 2014; Available at http://www.cantera.org.
[41] S.H. Won, B. Windom, B. Jiang, and Y. Ju, *The role of low temperature fuel chemistry on turbulent flame propagation*, Combust. Flame 161 (2014), pp. 475–483.
[42] S.H. Chung, *Stabilization, propagation and instability of tribrachial triple flames*, Proc. Combust. Inst. 31 (2007), pp. 877–892.
[43] Y.-S. Ko, T.-M. Chung, and S.-H. Chung, *Characteristics of propagating tribrachial flames in counterflow*, KSME Int. J. 16 (2002), pp. 1710–1718.
[44] N. Peters, P. Terhoeven, J.H. Chen, and T. Echekki, *Statistics of flame displacement speeds from computations of 2-D unsteady methane–air flames*, Symp. (Int.) Combust. 27 (1998), pp. 833–839.

Downloaded by [Lund University Libraries] at 01:40 25 November 2015